Engineering Computations

A binary-tree subdivision method for evaluation of singular integrals with discontinuous kernel in 3D BEM

Chuanming Ju
Peking University, Beijing, China and Yantai University, Yantai, China
Jiehao Chen
Yantai University, Yantai, China
Ning Li
Triangle Tyre Co Ltd, Weihai, China, and
Xianfeng Du
Yantai University, Yantai, China

Received 12 May 2024
Revised 16 July 2024
Accepted 20 September 2024

Abstract

Purpose – A binary-tree subdivision method (BTSM) for numerical evaluation of weakly singular integrals with discontinuous kernel in the three-dimensional (3D) boundary element method (BEM) is presented in this paper.
Design/methodology/approach – In this method, the singular boundary element is split into two sub-elements and subdivided recursively until the termination criterion is met and the subdivision is stopped. Then, the source point is surrounded by one or more spherical cavities determined by the discontinuous kernel function. The sub-elements located in spherical cavities will be eliminated, and the regular triangular or rectangle elements are employed to fill the spherical cavities.
Findings – With the proposed method, the obtained sub-elements are automatically refined as they approach the source point, and they are "good" in shape and size for standard Gaussian quadrature. Thus, the proposed method can be used to evaluate singular integrals owing discontinuous kernel function accurately for cases of different element shapes and various source point locations.
Originality/value – Numerical examples show that the BTSM is suitable for planar and curved elements of arbitrary regular or irregular shape at various source point locations, and the results have much better accuracy and robustness than conventional subdivision method (CSM) when the kernel function is discontinuous.

Keywords Singular integrals, Element subdivision, Discontinuous functions, Binary-tree
Paper type Research paper

1. Introduction

The boundary element method (BEM) is effective for solving partial differential equations, which can be transformed into boundary integral equations. These equations are often singular, sometimes even hyper singular. The singular integral equation has various applications in various disciplines, such as mathematical physics, fluid mechanics (Luo *et al.*, 2012; Chen *et al.*, 2015), fracture mechanics (Chen, 2004; Li *et al.*, 1998; Sukulthanasorn *et al.*, 2023), quantum mechanics, electromagnetism, electrostatics and other disciplines. In BEM, the kernel function of singular integrals is generally divided into continuous and discontinuous functions. For the transient heat conduction problem (Zhou *et al.*, 2015) with a fundamental solution in the time domain, the integrand is a regular continuous function in the whole defined domain; For transient elastic dynamics problem (Ma *et al.*, 2007) or physical problems such as electromagnetic waves and seismic waves, the integrand is discontinuous at some points and the conventional Gaussian integral or Hammer–Stroud integral criterion is invalid

This work was supported by Shandong Provincial Natural Science Foundation of China (Grant Number: ZR2022QA072), Yantai Science and Technology Bureau (Grant Number: 2023XDRH002) and China Postdoctoral Science Foundation under (Grant Number: 2024M761755).

Engineering Computations

0264-4401
DOI 10.1108/EC-05-2024-0400

(Pin and Haibo, 2005; Kosinka and Bartoň, 2019; Bartoň and Calo, 2016). It is impossible to calculate the singular integral with the integral as discontinuous accurately.

Up to now, there have been numerous efforts to eliminate or solve the singularities appearing in boundary integral equations. Brebbia *et al*. (2012) proposed the logarithmic integral formula to solve the logarithmic singular integral for plane problems, but this method has strict requirements for the form of the integrand, so its universality is poor. The rigid body displacement method (Chen *et al*., 1998) utilizes the special solution of the boundary integral equation to transform strong singular integrals into regular integrals, thereby indirectly calculating strong singular integrals. Liu and Rudolphi (1991, 1999), Liu (2000) proposed a series of integral identities, which were employed to regularize hyper singular boundary integral equations into boundary integral equations with only weak singularity. However, this method is not suitable for evaluating singular integrals in crack problems. Rungamornrat and Mear (2008a, b, 2011, 2019), Hu and Mear (2022) proposed the symmetric Galerkin boundary element method (SGBEM) which is based upon a weak-form boundary integral equation and implemented in a general framework allowing the treatment of material anisotropy and cracks of arbitrary shapes and under general loading conditions. Guiggiani (1998) proposed the local coordinate approximation expansion method, which solves strong singular integrals and hyper singular integrals in BEMs. Of course, there are also many other methods (Gao, 2010; Ma and Kamiya, 2003) to evaluate singular integrals. Among the above methods, the local coordinate transformation method has good universality and is suitable for different types of singular integrals. However, the computational accuracy of this method is affected by the shape of the integral element and the position of the source point. When the shape of the element is poor or the position of the source point relative to the integral element is biased, the accuracy of the integration calculation sharply decreases. The main reason is that this method subdivides singular elements by directly connecting its vertexes and the source point. When the source point is close to the boundary of the singular element, the shape of the patches obtained by subdivision is poor.

To solve this problem, element subdivision (Klees, 1996; Gao *et al*., 2008; Zhang *et al*., 2015, 2019a) is one of the most widely used methods for evaluating singular integral. In the conventional subdivision method (CSM), the sub-elements, also called patches, are obtained by simply connecting the singular point with each vertex of the element (Klees, 1996), as shown in Figure 1. However, in the CSM, the accuracy of evaluating singular integrals owing discontinuous kernel function cannot satisfy the demand for numerical simulation, as shown in Table 1. Moreover, when the elements are distorted or irregularly shaped, the shape of the patches obtained by the CSM will also be irregular, resulting in low integration accuracy. Zhang *et al*. (2015) proposed the spherical subdivision method which is not subdivided in the local coordinate system but in the physical coordinate system. An element is subdivided into a number of patches through a sequence of spheres with decreasing radius, and the obtained patches are automatically refined as they approach the source point. Each patch is “good” in

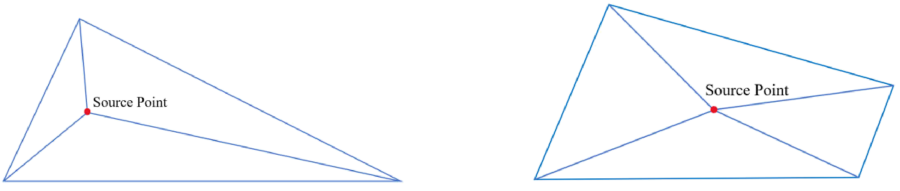

Source(s): Created by authors

Figure 1. Patches obtained by the conventional subdivision method

Table 1. Integral accuracy obtained by conventional subdivision method

Gaussian points number Patches (Figure 1(a))	Patches (Figure 1(b))	Relative error Patches (Figure 1(a))	Patches (Figure 1(b))
185	177	1.5473e−002	7.5015e−003
521	505	8.9529e−003	1.2620e−002
644	758	1.6589e−003	2.5988e−003
883	933	2.3423e−003	3.0095e−003

Source(s): Created by authors

shape and size for standard Gaussian quadrature integration. However, this method does not guarantee the convergence of the element subdivision.

In order to accurately and efficiently calculate the singular integral with discontinuous function, the paper proposes a binary-tree subdivision method (BTSM) based on the idea of dichotomy. The method divides the element in half and subdivides it recursively until the termination condition is met and the subdivision is stopped. According to the discontinuity points of kernel function, this method will generate spherical cavities to isolate the source points. The patches inside the spherical cavities are then eliminated, and the cavities are filled with regular triangular or rectangle patches. Thus, the shape of patches closer to the source point is relatively regular.

The rest of the paper is organized as follows: Section 2 describes the singular integrals with discontinuous kernel function. The details of the BTSM are discussed in Section 3 and 4. Section 5 provides some numerical examples which compare the proposed method with the CSM. In Section 6, the paper ends with conclusions.

2. The singular integral equation with discontinuous kernel function

An important step in the implementation of the BEM is the evaluation of various integrals containing kernel functions of the type $1/r^p$, where r is the distance between the evaluation point (also called source point) and the field point, and p represents the order of the singularity (Brebbia *et al.*, 2012; Provatidis, 1998; Gao and Davies, 2000). For any given integral domain S, the singular integral equation with a discontinuous function is as follows:

$$I = \begin{cases} \int_{S_0} f_0(r) N dS, & r \le R_0; \\ \int_{S_1} f_1(r) N dS, & R_0 < r \le R_1; \\ \vdots \\ \int_{S_n} f_n(r) N dS, & r > R_{n-1}; \end{cases} \tag{1}$$

where r is the distance from the source point to the field point, $f_i(r)$ is the discontinuous kernel function, and N is the element shape function. An integral equation with a discontinuous kernel function (Zhang *et al.*, 2019b) is shown in Formula(2), and its discontinuous function is depicted graphically in Figure 2.

$$I = \begin{cases} \int_{S_0} \frac{1}{r^2} N dS, & r \le 0.2; \\ \\ \int_{S_1} \frac{1}{2r^2} N dS, & r > 0.2; \end{cases} \tag{2}$$

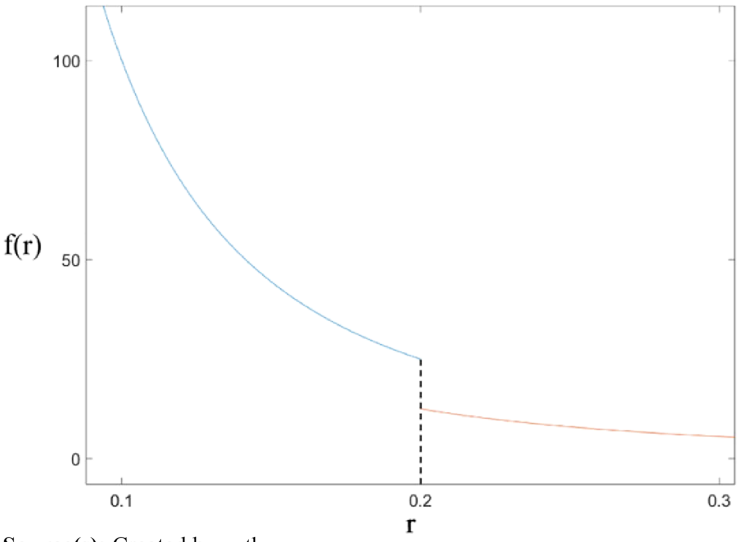

Source(s): Created by authors

Figure 2. The graph of the discontinuous kernel in Formula (2)

3. Binary tree subdivision algorithm for singular integral with discontinuous kernel functions

The binary tree subdivision algorithm adopts the idea of dichotomy, which first subdivides a singular element into two sub-elements called by patches. Then, the patches will be evaluated whether it meets the conditions for further subdivision. If the patches meet the subdivision conditions, they will continue to be subdivided until they do not meet the subdivision conditions. The patches closed to the source point will be deleted and new patches will be generated based on the feature sphere whose position is determined by the discontinuous point of the kernel function. The details of the binary tree subdivision algorithm are described below.

3.1 The feature sphere determined by discontinuous kernel functions

When the kernel function is discontinuous, the radius of the feature sphere is determined by the discontinuous point of this function. As shown in Figure 3, a function has two discontinuity points (at $r = R_0$ and R_1), and the radius of two feature spheres is R_0 and R_1, respectively. The singular integral element in Figure 3 can be isolated into three different regions, and the regions will be filled by the patches.

3.2 Subdivision criterion

In Figure 4, S is the source point, R_C is the radius of the maximum feature sphere, O is the center of the circumscribed circle of a patch, R is the radius of the circumscribed circle of the patch, and L is the distance from O to S. A subdivision radio ε is set, and its value can determine which integral patches need to be subdivided. When $L/R < \varepsilon$, the patch is considered to be close enough to the source point, that is, the patch meets the subdivision criterion, and the patch will be subdivided into two new patches. On the contrary, when $L/R \geq \varepsilon$, it means that the patch is far away from the source point, and the size of the circumscribed circle radius R of the patch and the radius R_C need to be further compared. Considering the difference in the number of patches obtained by subdivision when ε takes different values, the integration accuracy and efficiency are generally better when ε takes about 0.8 according to experience. Figure 5 shows the flow chart of the subdivision conditions.

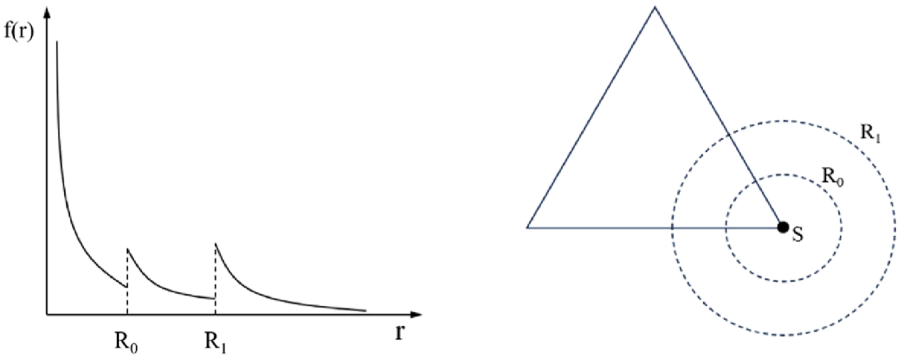

Source(s): Created by authors

Figure 3. Discontinuity points and radius of feature sphere

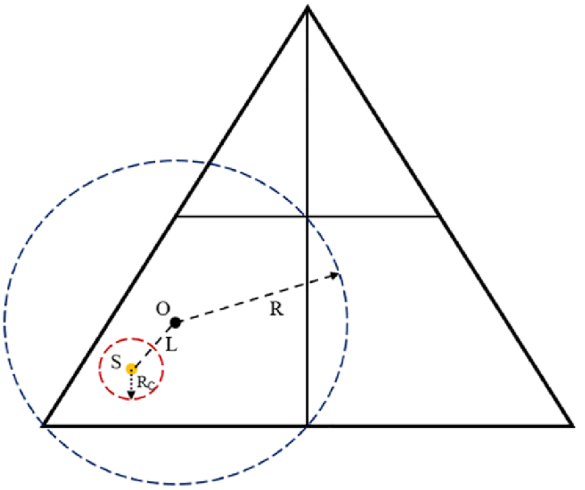

Source(s): Created by authors

Figure 4. Distance-based element subdivision criterion

3.3 The formation of the cavity

Once the initial subdivision of the integral element is complete, the patches whose edges intersect or are tangent to the feature sphere are removed to form cavity, as shown in Figure 6(a, b). To ensure the shape of obtained patches is more regular, the cavity should be adjusted to ensure that the cavity is not concave, as shown in Figure 6(c). In order to improve the calculation accuracy, the cavity should be adjusted again to ensure that the cavity is not concave, as shown in Figure 6(c).

3.4 The radial patches filling the cavity

There are three steps in generating radial patches: Firstly, projecting the points on the cavity along the radius direction of the feature sphere to obtain the projection point P_0 on the feature sphere; Secondly, connecting the points on the cavity and the projection points to form external radial patches located between the feature sphere and the cavity. At last, connecting the

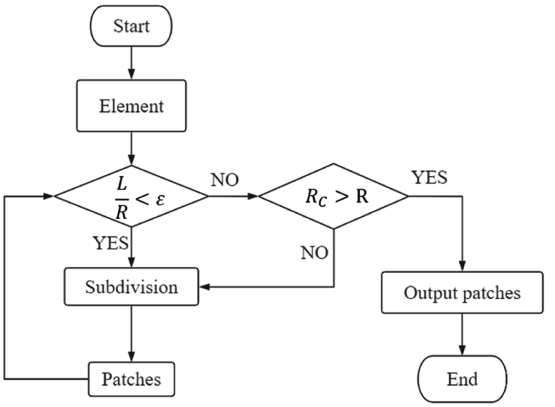

Source(s): Created by authors

Figure 5. Flow diagram of initial subdivision algorithm

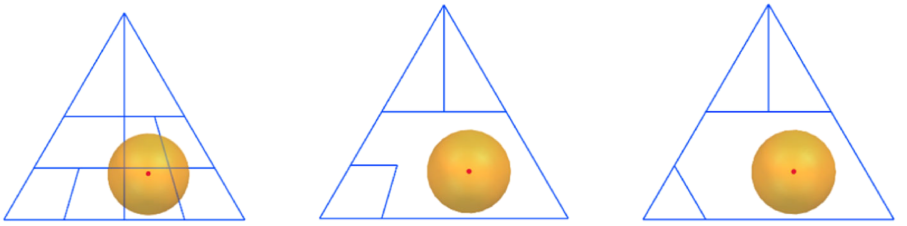

(a) **(b)** **(c)**

Source(s): Created by authors

Figure 6. The process of forming a cavity

projection points with the source point to generate the internal radial patches, as shown in Figure 7(a).

For the case of multiple feature spheres, the implementation of two feature spheres is taken as an example. Firstly, projecting the point P_1 on the inner feature sphere along the radius direction of outer feature sphere to get the projection point P_0; Secondly, connecting the points on the outer sphere and the points on the inner sphere to form the radial patches located between two feature spheres, as shown in Figure 7(b), Lastly, connecting the points on inner sphere with the source point to form the internal radial patches, as shown in Figure 7(c). The output patches are shown in Figure 8.

4. Four-node serendipity triangular patch

In the BTSM, the obtained patches around the source point are called by the four-node serendipity triangular patches proposed by Zhang *et al.* (2019a), Zhong *et al.* (2016). These serendipity patches require fewer sample points to obtain higher integration accuracy. A typical serendipity triangular patch is as shown in Figure 9 where the distance $\overline{01}$ and the distance $\overline{03}$ are equal to the radius of the feature sphere.

To resolve the singularity at point 0, a local coordinate transformation is employed, as shown in Figure 10.

Consider the following integral over the patch surface S:

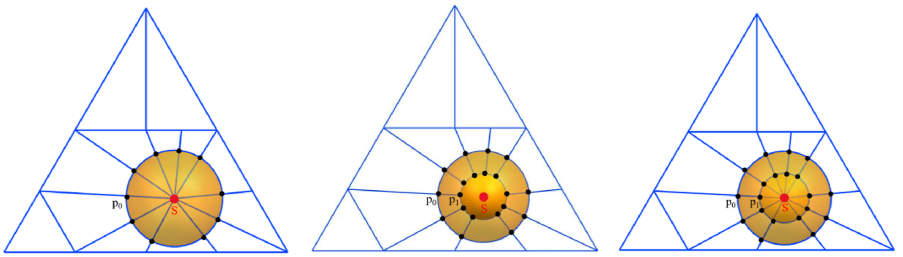

(a) **(b)** **(c)**

Source(s): Created by authors

Figure 7. The radial patches

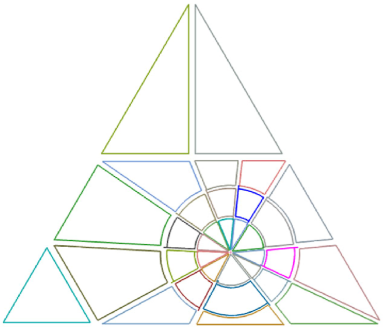

Source(s): Created by authors

Figure 8. The output patches

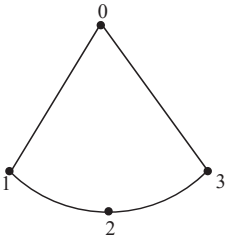

Source(s): Created by authors

Figure 9. Four-node serendipity triangular patch

$$I(\xi) = \int_S \frac{f(x,\xi)}{|x-\xi|} N(x) dS(x) \tag{3}$$

Here ξ refers to the singular point (x_0, y_0), $\boldsymbol{x}$ refers to a field point (x, y), $|x-\xi|$ represents the distance between a field point and the singular point hence weakly singular at point $0, f(x,\xi)$ is a well-behaved function, and $N(x)$ is a shape function.

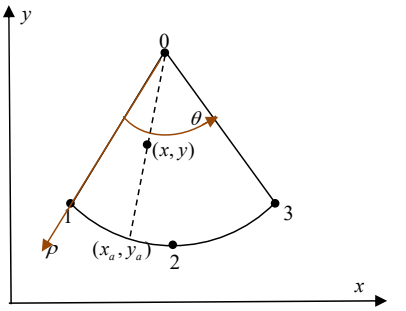

Source(s): Created by authors

Figure 10. The coordinate transformation of serendipity triangular patch

For this patch, a coordinate transformation in terms of a local coordinate ρ and a local coordinate θ can be written as follows:

$$\begin{cases} x = x_0 + (x_a - x_0)\rho \\ y = y_0 + (y_a - y_0)\rho \end{cases} \quad \because \rho \in [0, 1] \tag{4}$$

Such that the field points on the arch $\overset{\frown}{123}$ are interpolated as follows:

$$\begin{cases} x_a = N_1(\theta)x_1 + N_2(\theta)x_2 + N_3(\theta)x_3 \\ y_a = N_1(\theta)y_1 + N_2(\theta)y_2 + N_3(\theta)y_3 \end{cases} \quad \because \theta \in [-1, 1] \tag{5}$$

where $N_1(\theta)$, $N_2(\theta)$, and $N_3(\theta)$ are quadratic shape functions to approximate the arch $\overset{\frown}{123}$ as a parabola. Then the integral $I(\xi)$ can be written as follows:

$$I(\xi) = \int_{-1}^{1} \int_{0}^{1} \frac{f(x, \xi)}{|x - \xi|} N(x) J(\rho, \theta) d\rho d\theta \tag{6}$$

where $J(\rho, \theta)$ is the Jacobian of the transformation from the x-y system to the ρ-θ system, such that:

$$J(\rho, \theta) = \rho \left[(x_a - x_0) \frac{\partial y_a}{\partial \theta} - (y_a - y_0) \frac{\partial x_a}{\partial \theta} \right]. \tag{7}$$

And the derivation details for Formula (7) are presented in literature (Zhong *et al.*, 2016).

The weak singularity in the integral $I(\xi)$ is removed by the implementation of this transformation as the Jacobian in Formula (7) introduces the local coordinate ρ in the numerator. It can also be noted that this new coordinate system transformation is much simpler to implement than the conventional polar coordinate system in Telles (1987), as the local coordinates ρ and θ are automatically constrained to the intervals $[0, 1]$ and $[-1, 1]$ respectively, rendering the four-node serendipity triangular patch computationally more efficient (Zhang *et al.*, 2019a; Zhong *et al.*, 2016).

5. Numerical examples

In order to verify the accuracy and efficiency of the proposed method, the singular integral with discontinuous kernel function is evaluated, and the integral element includes planar and curved elements, respectively. The discontinuous kernel functions are expressed in

Formula (8) and (9), and their graphics are shown in Figure 11. The relative error is calculated by Formula (10) to get the accuracy of the proposed method and the CSM (Telles, 1987).

$$I = \begin{cases} \int_S \frac{1}{4r} dS, & r \le 1; \\ \int_S \frac{1}{r} dS, & r > 1; \end{cases} \tag{8}$$

$$I = \begin{cases} \int_S \frac{1}{2r} dS, & r \le 0.6; \\ \int_S \frac{1}{r} dS, & 0.6 < r \le 1; \\ \int_S \frac{2}{r} dS, & r > 1; \end{cases} \tag{9}$$

$$e_r = \left| \frac{I_e - I}{I} \right| \tag{10}$$

where r is the distance from the source point to the field point in any given integral domain S, I_e is the exact solution of the singular domain integral, and I is the numerical solution of the singular integral.

In all numerical examples the non-singular triangular and quadrilateral patches that are evaluated by standard Gaussian and Hammer quadrature integration, respectively. The number of Gaussian points m (Gao and Davies, 2000; Bu and Davies, 1995; Lachat and Watson, 1976) is determined by the following relation:

$$m = -\frac{1}{10} \ln\left(\frac{e}{2}\right) \sqrt{\frac{2}{3}p + \frac{2}{5}} \left[\left(\frac{8L}{3R}\right)^{\frac{3}{4}} + 1 \right] \tag{11}$$

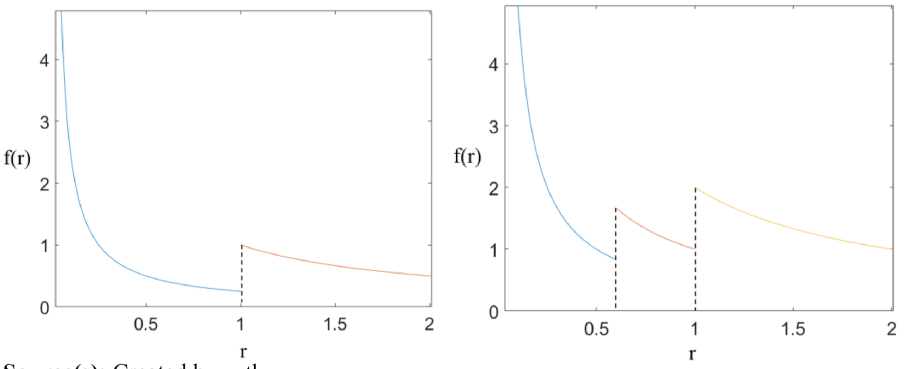

Source(s): Created by authors

Figure 11. Graphics of discontinuous kernel functions

EC

where p represents the order of the singularity ($p = 1, 2, 3$), e denotes the error tolerance, L is the length of the patch in the integral direction and R is the minimum distance from the source point to the boundary element.

5.1 Planar elements

This section gives some numerical examples for planar elements including regular, slender and obtuse elements *et al*. The subdivision results and calculation accuracy for different integral elements and kernel functions are described in following sections.

5.1.1 Planar triangular elements. The following numerical examples include planar triangular elements with regular, slender and obtuse triangular shapes. In the physical coordinate system, the vertex coordinates of the regular triangular element are (0,0,0), (10,0,0), (5,8.6,0), while the vertex coordinates of the slender triangular element are (0,0,0), (4.5,0,0), (2,16,0) and the vertex coordinates of the obtuse triangular element are (0,0,0), (12,0,0), (18,4,0). Based on different kernel functions, Figures 12–20 show the subdivisions for different triangular elements with various locations of source points. Tables 2–19 show the

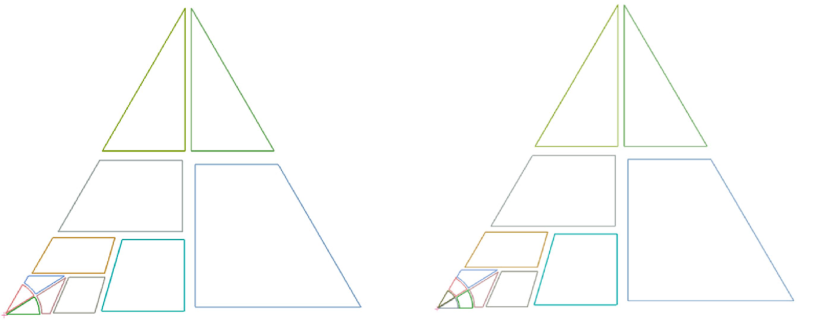

(a) **(b)**

Source(s): Created by authors

Figure 12. Subdivision of a regular triangular element with source point at the vertex of element: (a) The discontinuous kernel function is Formula (8), (b) The discontinuous kernel function is Formula (9)

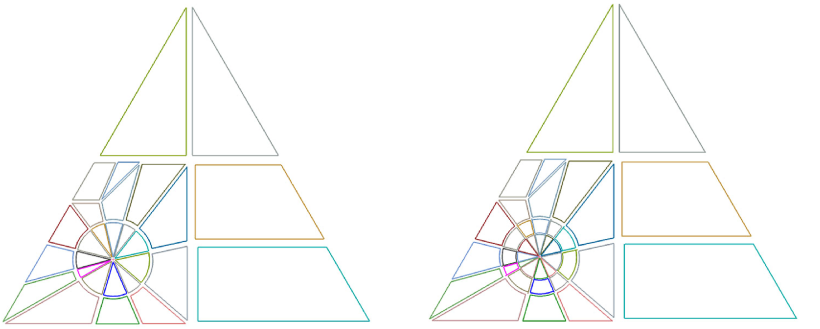

(a) **(b)**

Source(s): Created by authors

Figure 13. Subdivision of a regular triangular element with source point at the interior of element: (a) The discontinuous kernel function is Formula (8), (b) The discontinuous kernel function is Formula (9)

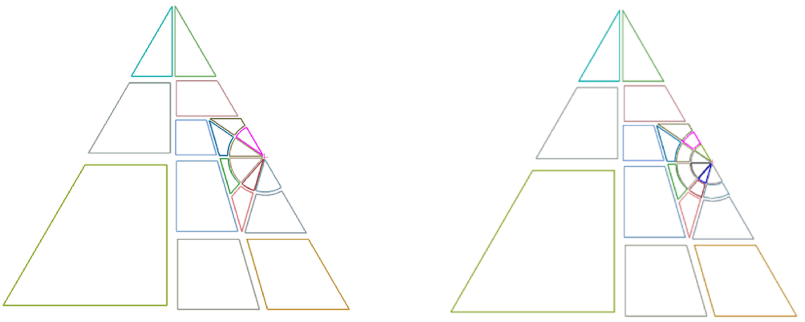

(a) (b)

Source(s): Created by authors

Figure 14. Subdivision of regular triangular element with source point at the edge of element: (a) The discontinuous kernel function is Formula (8), (b) The discontinuous kernel function is Formula (9)

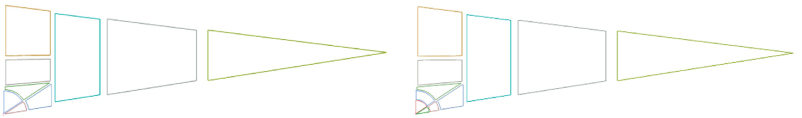

(a) (b)

Source(s): Created by authors

Figure 15. Subdivision of a slender triangular element with source point at the vertex of element: (a) The discontinuous kernel function is Formula (8), (b) The discontinuous kernel function is Formula (9)

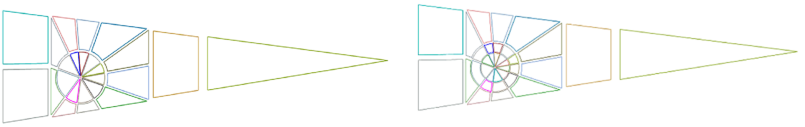

(a) (b)

Source(s): Created by authors

Figure 16. Subdivision of a slender triangular element with source point at the interior of element: (a) The discontinuous kernel function is Formula (8), (b) The discontinuous kernel function is Formula (9)

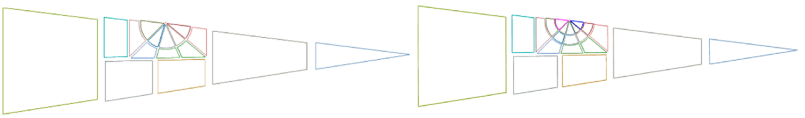

(a) (b)

Source(s): Created by authors

Figure 17. Subdivision of a slender triangular element with source point at the edge of element: (a) The discontinuous kernel function is Formula (8), (b) The discontinuous kernel function is Formula (9)

(a) **(b)**

Source(s): Created by authors

Figure 18. Subdivision of an obtuse triangular element with source point at the vertex of element: (a) The discontinuous kernel function is Formula (8), (b) The discontinuous kernel function is Formula (9)

(a) **(b)**

Source(s): Created by authors

Figure 19. Subdivision of an obtuse triangular element with source point at the interior of element: (a) The discontinuous kernel function is Formula (8), (b) The discontinuous kernel function is Formula (9)

(a) **(b)**

Source(s): Created by authors

Figure 20. Subdivision of an obtuse triangular element with source point at the edge of element: (a) The discontinuous kernel function is Formula (8), (b) The discontinuous kernel function is Formula (9)

Table 2. Numerical evaluation of singular integral (kernel function is Formula (8)) for a regular triangular element with source point at the vertex of element

Planar element	Source point	Gaussian points number		Relative error	
		CSM	BTSM	CSM	BTSM
Regular triangular element	(0,0)	54	54	5.2020e−002	1.5296e−003
		72	72	5.2020e−002	1.2521e−004
		133	133	2.0160e−002	3.2295e−005
		192	192	3.3633e−002	2.9325e−005
		260	260	1.6878e−002	3.0703e−005
		336	336	1.8459e−003	3.0817e−005

Source(s): Created by authors

accuracy obtained by the BTSM and the CSM for singular integral whose integrand are Formula (8) and (9).

As can be seen from the results shown in the Figures 12–20, based on different discontinuous functions, the patches around the source point are regular. The distribution of patches closed to the source point is dense, and the distribution of patches far away from the source point is sparse. Tables 2–19 reveal that the BTSM can exhibit the same level of accuracy

Table 3. Numerical evaluation of singular integral (kernel function is Formula (9)) for a regular triangular element with source point at the vertex of element

Planar element	Source point	Gaussian points number CSM	Gaussian points number BTSM	Relative error CSM	Relative error BTSM
Regular triangular element	(0,0)	58	58	1.6444e−002	1.5135e−003
		84	84	1.8462e−002	1.2706e−004
		145	145	8.0382e−003	2.9193e−005
		213	213	1.7959e−002	2.6256e−005
		284	284	4.2351e−003	2.7614e−005
		372	372	4.0291e−003	2.7727e−005

Source(s): Created by authors

Table 4. Numerical evaluation of singular integral (kernel function is Formula (8)) for a regular triangular element with source point at the interior of element

Planar element	Source point	Gaussian points number CSM	Gaussian points number BTSM	Relative error CSM	Relative error BTSM
Regular triangular element	(0.2,0.2)	129	129	1.6568e−003	1.4875e−003
		196	196	1.3734e−002	3.5527e−005
		335	335	3.0692e−002	6.4727e−005
		524	524	3.6395e−003	6.9744e−005
		648	648	2.8498e−004	6.9649e−005
		906	906	5.3527e−003	6.9745e−005

Source(s): Created by authors

Table 5. Numerical evaluation of singular integral (kernel function is Formula (9)) for a regular triangular element with source point at the interior of element

Planar element	Source point	Gaussian points number CSM	Gaussian points number BTSM	Relative error CSM	Relative error BTSM
Regular triangular element	(0.2,0.2)	153	153	1.0459e−002	1.4374e−003
		256	256	4.4677e−003	2.3341e−005
		427	427	6.0746e−003	5.7032e−005
		647	647	6.3251e−004	6.1975e−005
		815	815	2.7484e−003	6.1884e−005
		1,110	1,110	3.9809e−003	6.1973e−005

Source(s): Created by authors

as the CSM with fewer Gaussian integration points, and in addition, for the same number of Gaussian integration points, the BTSM has higher accuracy than the CSM and is able to achieve errors of 2–3 orders of magnitude lower in most cases.

5.1.2 Planar quadrilateral elements. In the following numerical examples, planar quadrilateral elements with regular, slender and irregular quadrilateral shapes are included. In the physical coordinate system, the vertex coordinates of regular quadrilateral element are (0,0,0), (6,0,0), (6,6,0), (0,6,0), the vertex coordinates of slender quadrilateral element are (0,0,0), (20,0,0), (20,3,0), (0,3,0) and the vertex coordinates of irregular quadrilateral element

Table 6. Numerical evaluation of singular integral (kernel function is Formula (8)) for a regular triangular element with source point at the edge of element

Planar element	Source point	Gaussian points number		Relative error	
		CSM	BTSM	CSM	BTSM
Regular triangular element	(0.5,0.5)	84	84	4.9938e−003	9.1206e−004
		129	129	3.2524e−002	1.8220e−005
		231	231	2.9263e−002	6.8054e−005
		340	340	5.6082e−003	6.6624e−005
		448	448	1.6968e−002	6.7298e−005
		608	608	1.2792e−002	6.7334e−005

Source(s): Created by authors

Table 7. Numerical evaluation of singular integral (kernel function is Formula (9)) for a regular triangular element with source point at the edge of element

Planar element	Source point	Gaussian points number		Relative error	
		CSM	BTSM	CSM	BTSM
Regular triangular element	(0.5,0.5)	96	96	2.8303e−003	9.0537e−004
		155	155	3.2586e−003	3.3598e−006
		282	282	1.5390e−002	5.5847e−005
		400	400	1.6866e−002	5.4534e−005
		536	536	3.1372e−004	5.5191e−005
		708	708	4.4057e−003	5.5225e−005

Source(s): Created by authors

Table 8. Numerical evaluation of singular integral (kernel function is Formula (8)) for a slender triangular element with source point at the vertex of element

Planar element	Source point	Gaussian points number		Relative error	
		CSM	BTSM	CSM	BTSM
Slender triangular element	(1,0)	47	47	6.7550e−002	1.7970e−003
		76	76	2.8147e−002	3.0241e−004
		106	106	2.8147e−002	7.4515e−005
		167	167	5.0901e−003	9.9327e−005
		224	224	2.1753e−002	1.0421e−004
		304	304	8.7240e−003	1.0424e−004

Source(s): Created by authors

are (0,0,0), (12,0,0), (8,6,0), (4,5,0). Figures 21–29 show the subdivisions for different quadrilateral elements with various locations of source points. Tables 20–37 show the accuracy obtained by the BTSM and the CSM for singular integral whose integrand are Formula (8) and (9).

Similar to planar triangular elements, the shape of patches obtained by BTSM for planar quadrilateral elements is regular, especially the patches near the source point. As can be illustrated from the Tables 20–37, whether the kernel function owns a discontinuous point or

Table 9. Numerical evaluation of singular integral (kernel function is Formula (9)) for a slender triangular element with source point at the vertex of element

Planar element	Source point	Gaussian points number CSM	BTSM	Relative error CSM	BTSM
Slender triangular element	(1,0)	52	52	1.2391e−002	1.7857e−003
		88	88	1.2756e−002	2.7783e−004
		127	127	4.5610e−003	6.1071e−005
		191	191	6.3320e−003	8.5721e−005
		264	264	1.2619e−002	9.0521e−005
		348	348	3.7595e−003	9.0549e−005

Source(s): Created by authors

Table 10. Numerical evaluation of singular integral (kernel function is Formula (8)) for a slender triangular element with source point at the interior of element

Planar element	Source point	Gaussian points number CSM	BTSM	Relative error CSM	BTSM
Slender triangular element	(0.5,0.2)	109	109	4.4672e−004	1.0764e−003
		168	168	9.5471e−003	1.8544e−004
		285	285	9.6033e−003	2.0234e−004
		431	431	1.5094e−003	2.2227e−004
		526	526	7.6436e−003	2.2322e−004
		745	745	5.5337e−003	2.2325e−004

Source(s): Created by authors

Table 11. Numerical evaluation of singular integral (kernel function is Formula (9)) for a slender triangular element with source point at the interior of element

Planar element	Source point	Gaussian points number CSM	BTSM	Relative error CSM	BTSM
Slender triangular element	(0.5,0.2)	130	130	1.4687e−002	1.0700e−003
		224	224	1.5828e−002	1.2867e−004
		381	381	3.6178e−006	1.6097e−004
		545	545	3.1522e−003	1.8078e−004
		695	695	2.0745e−003	1.8168e−004
		949	949	3.1243e−003	1.8169e−004

Source(s): Created by authors

two points, the BTSM can achieve the same level of accuracy as the CSM with fewer Gaussian integration points. Furthermore, for the same number of Gaussian integration points, the BTSM has higher accuracy than the CSM.

5.2 Curved elements

In this section, we give the results of the BTSM and its calculation accuracy when the integral elements are curved elements.

Table 12. Numerical evaluation of singular integral (kernel function is Formula (8)) for a slender triangular element with source point at the edge of element

Planar element	Source point	Gaussian points number		Relative error	
		CSM	BTSM	CSM	BTSM
Slender triangular element	(0,0.4)	73	73	3.4879e−002	2.2673e−003
		118	118	3.7224e−002	9.1060e−005
		201	201	9.9569e−003	9.4277e−006
		316	316	1.4770e−002	2.3299e−005
		399	399	2.3032e−003	2.3880e−005
		560	560	4.5590e−003	2.3923e−005

Source(s): Created by authors

Table 13. Numerical evaluation of singular integral (kernel function is Formula (9)) for a slender triangular element with source point at the edge of element

Planar element	Source point	Gaussian points number		Relative error	
		CSM	BTSM	CSM	BTSM
Slender triangular element	(0,0.4)	84	84	3.1904e−004	2.2182e−003
		146	146	2.5217e−002	1.0207e−004
		248	248	1.2257e−002	1.4254e−007
		376	376	1.4233e−003	1.3750e−005
		486	486	5.2244e−003	1.4315e−005
		656	656	5.1340e−003	1.4355e−005

Source(s): Created by authors

Table 14. Numerical evaluation of singular integral (kernel function is Formula (8)) for an obtuse triangular element with source point at the vertex of element

Planar element	Source point	Gaussian points number		Relative error	
		CSM	BTSM	CSM	BTSM
Obtuse triangular element	(1,0)	94	94	6.0139e−002	3.0441e−004
		149	149	4.9885e−003	2.3791e−004
		264	264	5.5496e−003	1.3276e−004
		385	385	1.3926e−002	1.2988e−004
		495	495	1.2370e−002	1.3118e−004
		668	668	6.5239e−003	1.3125e−004

Source(s): Created by authors

5.2.1 Curved triangular elements. In the following numerical examples, the coordinates of the physical coordinate system of the curved triangular elements are (0,0,0), (6,0,0), (2,16,0), and the coordinates of the midpoints of each edge are (3,0,1), (5,8,1.5), (1,8,1.5). Figures 30–32 show the subdivisions obtained by the BTSM for curved triangular element with different source points. Tables 38–43 show the accuracy obtained by the BTSM and the CSM for singular integral whose integrand are Formula (8) and (9), respectively.

For curved triangular element, no matter how many discontinuous intervals a discontinuous function has, the patches obtained by the BTSM are relatively regular around

Table 15. Numerical evaluation of singular integral (kernel function is Formula (9)) for an obtuse triangular element with source point at the vertex of element

Planar element	Source point	Gaussian points number CSM	Gaussian points number BTSM	Relative error CSM	Relative error BTSM
Obtuse triangular element	(1,0)	105	105	3.9092e−002	3.2294e−004
		175	175	4.1370e−003	2.0034e−004
		305	305	2.6724e−003	1.0744e−004
		436	436	7.7503e−003	1.0492e−004
		566	566	1.4710e−003	1.0618e−004
		756	756	5.5267e−003	1.0624e−004

Source(s): Created by authors

Table 16. Numerical evaluation of singular integral (kernel function is Formula (8)) for an obtuse triangular element with source point at the interior of element

Planar element	Source point	Gaussian points number CSM	Gaussian points number BTSM	Relative error CSM	Relative error BTSM
Obtuse triangular element	(0.5,0.3)	179	179	2.5220e−002	2.1712e−003
		267	267	2.3516e−002	3.2803e−005
		473	473	1.4219e−002	1.7130e−004
		711	711	7.0135e−003	1.7966e−004
		844	844	6.1620e−003	1.7998e−004
		1,190	1,190	3.6279e−003	1.8013e−004

Source(s): Created by authors

Table 17. Numerical evaluation of singular integral (kernel function is Formula (9)) for an obtuse triangular element with source point at the interior of element

Planar element	Source point	Gaussian points number CSM	Gaussian points number BTSM	Relative error CSM	Relative error BTSM
Obtuse triangular element	(0.5,0.3)	211	211	6.3747e−003	2.0717e−003
		343	343	3.6491e−003	5.0868e−006
		580	580	4.8774e−003	1.4042e−004
		861	861	3.1312e−004	1.4871e−004
		1,046	1,046	2.0061e−003	1.4899e−004
		1,434	1,434	2.8791e−003	1.4912e−004

Source(s): Created by authors

the source point, as can be illustrated from the Figures 30–32. From the Tables 38–43, it can be demonstrated that, for the same number of Gaussian integration points, the BTSM has higher accuracy than the CSM and is able to achieve errors of two orders of magnitude lower in most cases.

5.2.2 Curved quadrilateral element. In the following numerical example, the coordinates of the physical coordinate system of the curved quadrilateral elements are (0,0,0), (20,0,0), (20,3,0), (0,3,0). The coordinates of the midpoints of each edge are (10,0,1), (20,1.5,0.2), (10,3,1), (0,1.5,0.2). Figures 33–35 show the subdivisions obtained by the BTSM for curved

Table 18. Numerical evaluation of singular integral (kernel function is Formula (8)) for an obtuse triangular element with source point at the edge of element

Planar element	Source point	Gaussian points number CSM	Gaussian points number BTSM	Relative error CSM	Relative error BTSM
Obtuse triangular element	(0,0.5)	142	142	3.2068e−002	1.5275e−003
		220	220	9.0842e−003	5.5742e−005
		369	369	2.6925e−003	5.2313e−005
		551	551	1.4358e−003	5.7704e−005
		701	701	3.5640e−003	5.9782e−005
		983	983	2.4853e−003	5.9792e−005

Source(s): Created by authors

Table 19. Numerical evaluation of singular integral (kernel function is Formula (9)) for an obtuse triangular element with source point at the edge of element

Planar element	Source point	Gaussian points number CSM	Gaussian points number BTSM	Relative error CSM	Relative error BTSM
Obtuse triangular element	(0,0.5)	160	160	1.9693e−002	1.4865e−003
		260	260	6.0714e−003	4.0571e−005
		435	435	4.8096e−003	4.1946e−005
		626	626	7.6374e−003	4.7276e−005
		813	813	2.1435e−003	4.9269e−005
		1,115	1,115	1.9107e−003	4.9274e−005

Source(s): Created by authors

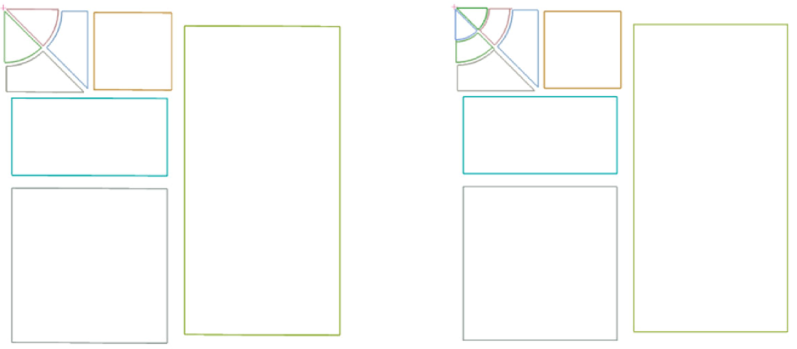

(a) **(b)**

Source(s): Created by authors

Figure 21. Subdivision of a regular quadrilateral element with source point at the vertex of element: (a) The discontinuous kernel function is Formula (8), (b) The discontinuous kernel function is Formula (9)

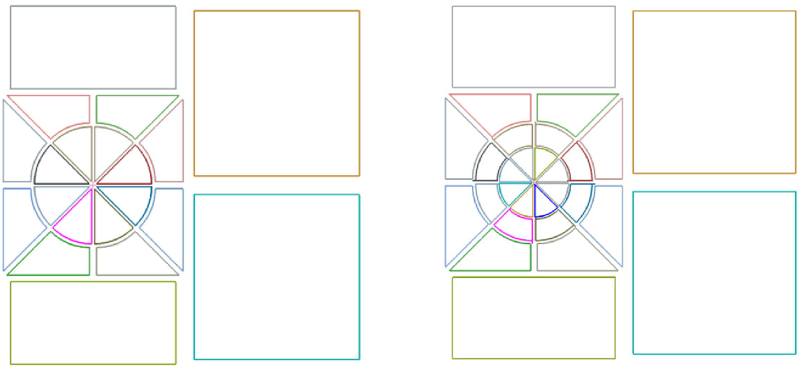

(a) (b)

Source(s): Created by authors

Figure 22. Subdivision of a regular quadrilateral element with source point at the interior of element: (a) The discontinuous kernel function is Formula (8), (b) The discontinuous kernel function is Formula (9)

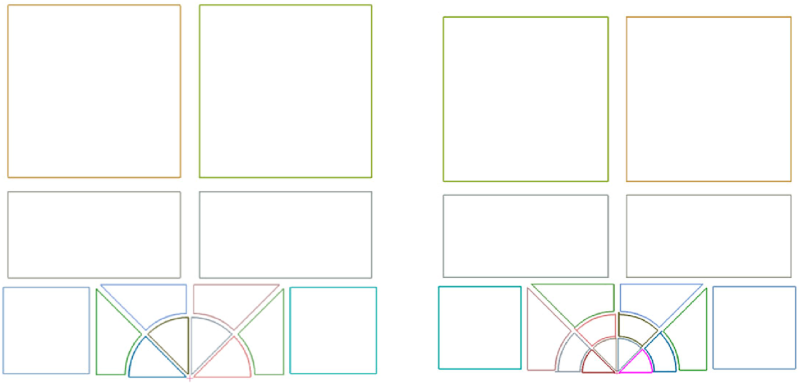

(a) (b)

Source(s): Created by authors

Figure 23. Subdivision of a regular quadrilateral element with source point at the edge of element: (a) The discontinuous kernel function is Formula (8), (b) The discontinuous kernel function is Formula (9)

quadrilateral element with different source points. Tables 44–47 show the accuracy obtained by the BTSM and the CSM for singular integral whose integrand are Formula (8) and (9), respectively.

As can be seen from the Figures 33–35, similar to the subdivision of curved triangular elements, the shape of patches subdivided by BTSM for the curved quadrilateral elements is regular, and especially the patches around the source point are composed by regular triangular or quadrangular elements. Tables 44–49 indicate that, no matter how many discontinuous points the kernel function has, the BTSM can achieve the same level of accuracy as the CSM with fewer Gaussian integration points. Furthermore, for the same number of Gaussian integration points, the BTSM has higher accuracy than the CSM.

(a)

(b)

Source(s): Created by authors

Figure 24. Subdivision of a slender quadrilateral element with source point at the vertex of element: (a) The discontinuous kernel function is Formula (8), (b) The discontinuous kernel function is Formula (9)

(a)

(b)

Source(s): Created by authors

Figure 25. Subdivision of a slender quadrilateral element with source point at the interior of element: (a) The discontinuous kernel function is Formula (8), (b) The discontinuous kernel function is Formula (9)

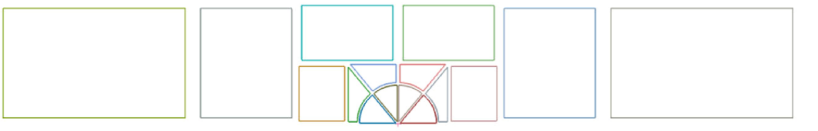

(a)

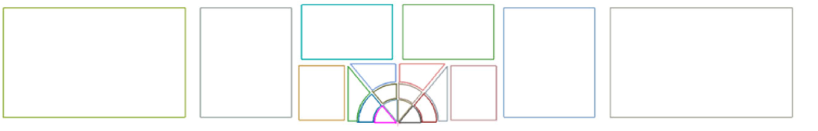

(b)

Source(s): Created by authors

Figure 26. Subdivision of a slender quadrilateral element with source point at the edge of element: (a) The discontinuous kernel function is Formula (8), (b) The discontinuous kernel function is Formula (9)

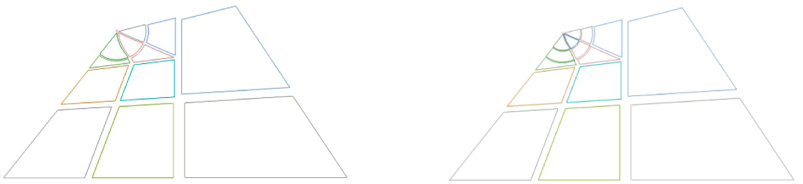

(a) (b)

Source(s): Created by authors

Figure 27. Subdivision of an irregular quadrilateral element with source point at the vertex of element: (a) The discontinuous kernel function is Formula (8), (b) The discontinuous kernel function is Formula (9)

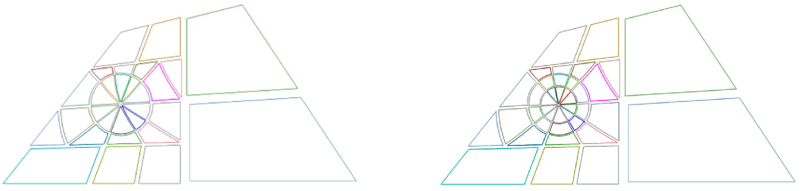

(a) (b)

Source(s): Created by authors

Figure 28. Subdivision of an irregular quadrilateral element with source point at the interior of element: (a) The discontinuous kernel function is Formula (8), (b) The discontinuous kernel function is Formula (9)

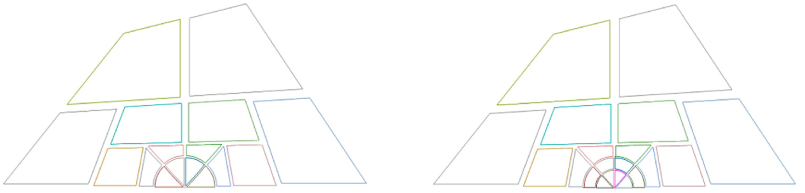

(a) (b)

Source(s): Created by authors

Figure 29. Subdivision of an irregular quadrilateral element with source point at the edge of element: (a) The discontinuous kernel function is Formula (8), (b) The discontinuous kernel function is Formula (9)

Table 20. Numerical evaluation of singular integral (kernel function is Formula (8)) for a regular quadrilateral element with source point at the vertex of element

Planar element	Source point	Gaussian points number		Relative error	
		CSM	BTSM	CSM	BTSM
Regular quadrilateral element	(−1,1)	44	44	1.0913e−001	1.7137e−003
		74	74	2.1428e−002	5.8456e−005
		96	96	2.5383e−002	4.6485e−005
		160	160	2.6979e−002	5.9364e−005
		212	212	1.1198e−002	6.6357e−005
		292	292	1.4835e−002	6.5333e−005

Source(s): Created by authors

Table 21. Numerical evaluation of singular integral (kernel function is Formula (9)) for a regular quadrilateral element with source point at the vertex of element

Planar element	Source point	Gaussian points number CSM	Gaussian points number BTSM	Relative error CSM	Relative error BTSM
Regular quadrilateral element	(−1,1)	50	50	3.7519e−002	1.6705e−003
		86	86	8.5223e−003	7.2519e−005
		116	116	3.5752e−002	5.6804e−005
		190	190	1.0947e−002	4.7390e−005
		247	247	3.7317e−003	5.4268e−005
		340	340	6.6133e−003	5.3260e−005

Source(s): Created by authors

Table 22. Numerical evaluation of singular integral (kernel function is Formula (8)) for a regular quadrilateral element with source point at the interior of element

Planar element	Source point	Gaussian points number CSM	Gaussian points number BTSM	Relative error CSM	Relative error BTSM
Regular quadrilateral element	(−0.5,0)	96	96	9.6541e−003	7.4119e−004
		130	130	2.6638e−003	8.4525e−005
		234	234	9.7579e−003	1.1170e−004
		374	374	1.4134e−002	1.1394e−004
		468	468	8.6227e−004	1.1658e−004
		650	650	1.0890e−002	1.1670e−004

Source(s): Created by authors

Table 23. Numerical evaluation of singular integral (kernel function is Formula (9)) for a regular quadrilateral element with source point at the interior of element

Planar element	Source point	Gaussian points number CSM	Gaussian points number BTSM	Relative error CSM	Relative error BTSM
Regular quadrilateral element	(−0.5,0)	120	120	5.1957e−003	7.3829e−004
		178	178	1.9493e−002	1.0753e−004
		322	322	4.5399e−003	9.0413e−005
		494	494	4.7389e−004	9.2766e−005
		618	618	8.6063e−003	9.5304e−005
		842	842	4.8322e−003	9.5413e−005

Source(s): Created by authors

5.3 The efficiency compared by BTSM and CSM

In this section, the efficiency of evaluating singular integral by BTSM and CSM is illustrated. The CPU time (in milliseconds) consumed by BTSM and CSM is counted on an Intel(R) Core (TM)i5-6600 3.3 GHz. And the test results are shown in Tables 50–53, where the time cost is reported by the total time running 1,000 times. In the BTSM, the implementation of subdivision is more complex than that of CSM, and the number of patches obtained by subdivision is larger than that of CSM, as shown in Figures 36 and 37. As shown in

Table 24. Numerical evaluation of singular integral (kernel function is Formula (8)) for a regular quadrilateral element with source point at the edge of element

Planar element	Source point	Gaussian points number CSM	Gaussian points number BTSM	Relative error CSM	Relative error BTSM
Regular quadrilateral element	(0, −1)	76	76	6.7424e−003	7.8062e−004
		124	124	2.6571e−002	1.0148e−005
		168	168	1.6771e−002	2.8774e−005
		280	280	2.0254e−002	8.7116e−005
		364	364	3.6433e−003	9.0814e−005
		500	500	1.1421e−003	9.0310e−005

Source(s): Created by authors

Table 25. Numerical evaluation of singular integral (kernel function is Formula (9)) for a regular quadrilateral element with source point at the edge of element

Planar element	Source point	Gaussian points number CSM	Gaussian points number BTSM	Relative error CSM	Relative error BTSM
Regular quadrilateral element	(0, −1)	88	88	8.5487e−004	7.3920e−004
		148	148	9.0601e−003	1.1739e−005
		212	212	4.9027e−003	1.2492e−005
		340	340	1.0182e−002	6.9487e−005
		439	439	4.8390e−003	7.3090e−005
		596	596	5.9879e−003	7.2598e−005

Source(s): Created by authors

Table 26. Numerical evaluation of singular integral (kernel function is Formula (8)) for a slender quadrilateral element with source point at the vertex of element

Planar element	Source point	Gaussian points number CSM	Gaussian points number BTSM	Relative error CSM	Relative error BTSM
Slender quadrilateral element	(−1,1)	48	48	2.8652e−002	9.1422e−004
		82	82	1.9125e−002	3.6707e−005
		129	129	6.9760e−003	8.6845e−005
		204	204	4.8413e−003	1.0009e−004
		273	273	4.1333e−003	1.0066e−004
		363	363	2.4736e−003	1.0067e−004

Source(s): Created by authors

Tables 50–53, for planer and curved element, the average time of CSM is 0.4 *ms* and the time required by BTSM increases as the number of Gaussian points increases. The minimum time required by CSM is significantly less than that of BTSM. Thus, the CPU time consumed by BTSM is larger than the total time consumed by CSM. However, the evaluation accuracy of BTSM is higher than that of CSM.

Table 27. Numerical evaluation of singular integral (kernel function is Formula (9)) for a slender quadrilateral element with source point at the vertex of element

Planar element	Source point	Gaussian points number CSM	Gaussian points number BTSM	Relative error CSM	Relative error BTSM
Slender quadrilateral element	(−1,1)	53	53	1.8432e−002	9.1570e−004
		94	94	8.0839e−003	1.7695e−005
		149	149	1.0394e−002	7.1346e−005
		231	231	5.8748e−003	8.4486e−005
		311	311	1.4008e−003	8.5046e−005
		407	407	7.9206e−004	8.5060e−005

Source(s): Created by authors

Table 28. Numerical evaluation of singular integral (kernel function is Formula (8)) for a slender quadrilateral element with source point at the interior of element

Planar element	Source point	Gaussian points number CSM	Gaussian points number BTSM	Relative error CSM	Relative error BTSM
Slender quadrilateral element	(−0.5,0)	106	106	7.7365e−003	2.4488e−003
		166	166	1.3710e−002	1.5857e−004
		302	302	8.6108e−003	1.4129e−004
		450	450	5.6778e−003	1.4861e−004
		559	559	1.1416e−002	1.5394e−004
		784	784	7.3039e−003	1.5445e−004

Source(s): Created by authors

Table 29. Numerical evaluation of singular integral (kernel function is Formula (9)) for a slender quadrilateral element with source point at the interior of element

Planar element	Source point	Gaussian points number CSM	Gaussian points number BTSM	Relative error CSM	Relative error BTSM
Slender quadrilateral element	(−0.5,0)	126	126	2.0274e−002	2.3792e−003
		214	214	3.7498e−003	1.8076e−004
		382	382	3.6316e−003	1.1791e−004
		558	558	6.4377e−003	1.2521e−004
		712	712	8.5544e−004	1.3033e−004
		960	960	2.1958e−003	1.3082e−004

Source(s): Created by authors

6. Conclusions

A BTSM for the accurate and efficient evaluation of weakly singular integrals whose kernel function is discontinuous in 3D BEM is implemented in this paper. When the integrand is discontinuous, or the shape of singular elements is irregular, the conventional Gaussian integral method usually has low calculation accuracy. In the BTSM, based on the number of discontinuous points of the kernel function, the source point can be isolated by one or more spherical cavities. The spherical cavities are filled by regular triangular or quadrangle

Table 30. Numerical evaluation of singular integral (kernel function is Formula (8)) for a slender quadrilateral element with source point at the edge of element

Planar element	Source point	Gaussian points number CSM	Gaussian points number BTSM	Relative error CSM	Relative error BTSM
Slender quadrilateral element	(0, −1)	80	80	5.4239e−003	9.2306e−004
		134	134	6.4469e−003	3.4673e−006
		216	216	1.2482e−003	6.0394e−005
		344	344	1.9152e−002	6.9181e−005
		456	456	9.0708e−003	6.9689e−005
		606	606	7.6008e−004	6.9704e−005

Source(s): Created by authors

Table 31. Numerical evaluation of singular integral (kernel function is Formula (9)) for a slender quadrilateral element with source point at the edge of element

Planar element	Source point	Gaussian points number CSM	Gaussian points number BTSM	Relative error CSM	Relative error BTSM
Slender quadrilateral element	(0, −1)	90	90	7.0177e−003	9.1436e−004
		158	158	7.8731e−003	1.6343e−005
		256	256	4.9496e−003	5.1695e−005
		398	398	6.2378e−003	6.0439e−005
		534	534	7.8772e−004	6.0938e−005
		694	694	3.3590e−003	6.0950e−005

Source(s): Created by authors

Table 32. Numerical evaluation of singular integral (kernel function is Formula (8)) for an irregular quadrilateral element with source point at the vertex of element

Planar element	Source point	Gaussian points number CSM	Gaussian points number BTSM	Relative error CSM	Relative error BTSM
Irregular quadrilateral element	(−1,1)	69	69	4.7141e−002	1.2050e−004
		107	107	7.9024e−004	4.3414e−005
		187	187	2.4618e−002	6.3347e−006
		279	279	1.9445e−003	7.2956e−006
		370	370	1.7735e−003	6.2775e−006
		476	476	4.9654e−004	6.3083e−006

Source(s): Created by authors

patches around the source point. The patches close to the source point are dense, and patches far away from the source point are sparse. Numerical examples demonstrate that, regardless of how many discontinuous points of the kernel function contains, the BTSM is suitable for planar or curved elements of arbitrary regular or irregular shape at various source point locations, and compared with the CSM, the accuracy and are significantly improved.

Table 33. Numerical evaluation of singular integral (kernel function is Formula (9)) for an irregular quadrilateral element with source point at the vertex of element

Planar element	Source point	Gaussian points number		Relative error	
		CSM	BTSM	CSM	BTSM
Irregular quadrilateral element	(−1,1)	76	76	7.9446e−003	1.0531e−004
		127	127	7.6465e−003	3.8425e−005
		223	223	1.1154e−003	3.7126e−007
		321	321	4.8396e−003	1.1700e−006
		438	438	8.5590e−004	1.6223e−007
		561	561	1.1092e−003	1.7299e−007

Source(s): Created by authors

Table 34. Numerical evaluation of singular integral (kernel function is Formula (8)) for an irregular quadrilateral element with source point at the interior of element

Planar element	Source point	Gaussian points number		Relative error	
		CSM	BTSM	CSM	BTSM
Irregular quadrilateral element	(−0.5,0)	128	128	1.5753e−002	9.3317e−004
		201	201	9.4336e−003	3.4250e−005
		355	355	6.6534e−003	6.8144e−005
		543	543	1.3086e−002	7.0447e−005
		671	671	4.3100e−003	7.0390e−005
		910	910	5.0703e−003	7.0414e−005

Source(s): Created by authors

Table 35. Numerical evaluation of singular integral (kernel function is Formula (9)) for an irregular quadrilateral element with source point at the interior of element

Planar element	Source point	Gaussian points number		Relative error	
		CSM	BTSM	CSM	BTSM
Irregular quadrilateral element	(−0.5,0)	151	151	3.5252e−003	9.0689e−004
		259	259	8.4781e−004	2.0989e−005
		454	454	9.0731e−004	5.5023e−005
		666	666	2.1957e−003	5.7400e−005
		847	847	8.3486e−004	5.7347e−005
		1,160	1,160	1.6959e−003	5.7375e−005

Source(s): Created by authors

Table 36. Numerical evaluation of singular integral (kernel function is Formula (8)) for an irregular quadrilateral element with source point at the edge of element

Planar element	Source point	Gaussian points number CSM	Gaussian points number BTSM	Relative error CSM	Relative error BTSM
Irregular quadrilateral element	(0, −1)	80	80	4.1091e−002	3.5253e−004
		136	136	2.9043e−002	4.0690e−004
		198	198	2.8904e−003	5.1590e−005
		312	312	1.1991e−002	8.2419e−005
		416	416	1.9256e−002	8.2943e−005
		587	587	1.8022e−002	8.3648e−005

Source(s): Created by authors

Table 37. Numerical evaluation of singular integral (kernel function is Formula (9)) for an irregular quadrilateral element with source point at the edge of element

Planar element	Source point	Gaussian points number CSM	Gaussian points number BTSM	Relative error CSM	Relative error BTSM
Irregular quadrilateral element	(0, −1)	90	90	1.8578e−002	3.6645e−004
		160	160	1.9977e−002	3.7218e−004
		246	246	9.0184e-003	2.7990e−005
		366	366	1.1280e−002	5.8344e−005
		496	496	7.2107e−003	5.8858e−005
		707	707	8.3424e−003	5.9548e−005

Source(s): Created by authors

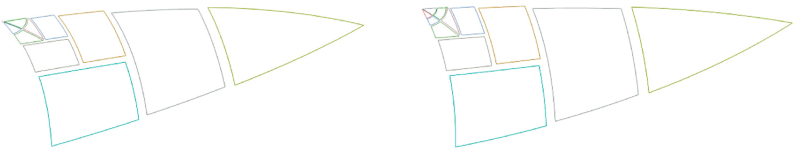

(a) **(b)**

Source(s): Created by authors

Figure 30. Subdivision of a curved triangular element with source point at the vertex of element: (a) The discontinuous kernel function is Formula (8), (b) The discontinuous kernel function is Formula (9)

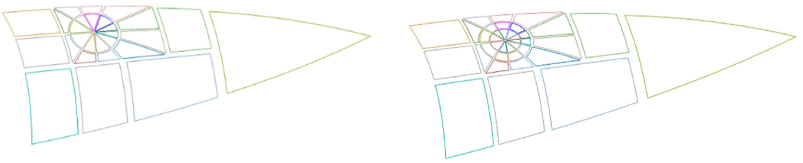

(a) **(b)**

Source(s): Created by authors

Figure 31. Subdivision of a curved triangular element with source point at the interior of element: (a) The discontinuous kernel function is Formula (8), (b) The discontinuous kernel function is Formula (9)

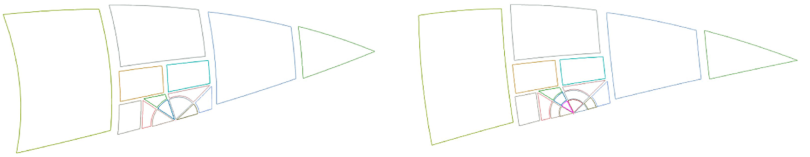

(a) **(b)**

Source(s): Created by authors

Figure 32. Subdivision of a curved triangular element with source point at the edge of element: (a) The discontinuous kernel function is Formula (8), (b) The discontinuous kernel function is Formula (9)

Table 38. Numerical evaluation of singular integral (kernel function is Formula (8)) for a curved triangular element with source point at the vertex of element

Curved surface element	Source point	Gaussian points number		Relative error	
		CSM	BTSM	CSM	BTSM
Triangular element	(0,0)	49	49	3.4875e−002	4.2611e−004
		66	66	3.4875e−002	3.1624e−004
		115	115	1.8325e−002	5.9532e−004
		174	174	4.6154e−003	5.9988e−004
		244	244	4.6632e−003	6.0182e−004
		306	306	5.0220e−003	6.0187e−004

Source(s): Created by authors

Table 39. Numerical evaluation of singular integral (kernel function is Formula (9)) for a curved triangular element with source point at the vertex of element

Curved surface element	Source point	Gaussian points number		Relative error	
		CSM	BTSM	CSM	BTSM
Triangular element	(0,0)	59	59	3.4024e−002	9.5991e−005
		78	78	1.0601e−002	6.3770e−004
		136	136	6.8714e−003	9.1572e−004
		201	201	1.2146e−003	9.2025e−004
		280	280	5.1923e−003	9.2218e−004
		356	356	2.6329e−003	9.2222e−004

Source(s): Created by authors

Table 40. Numerical evaluation of singular integral (kernel function is Formula (8)) for a curved triangular element with source point at the interior of element

Curved surface element	Source point	Gaussian points number		Relative error	
		CSM	BTSM	CSM	BTSM
Triangular element	(0.2,0.2)	125	125	1.1839e−002	1.3337e−003
		202	202	9.2187e−003	4.0762e−005
		354	354	3.5586e−003	9.9496e−006
		537	537	1.0101e−004	6.1148e−007
		664	664	4.2790e−003	2.0431e−007
		924	924	7.0063e−004	3.3597e−007

Source(s): Created by authors

Table 41. Numerical evaluation of singular integral (kernel function is Formula (9)) for a curved triangular element with source point at the interior of element

Curved surface element	Source point	Gaussian points number CSM	Gaussian points number BTSM	Relative error CSM	Relative error BTSM
Triangular element	(0.2,0.2)	157	157	1.0196e−003	1.2876e−003
		258	258	3.0321e−003	3.8995e−005
		459	459	7.5219e−004	3.6665e−006
		669	669	2.8045e−003	5.4894e−006
		844	844	2.4492e−003	6.2788e−006
		1,174	1,174	6.1370e−004	6.4038e−006

Source(s): Created by authors

Table 42. Numerical evaluation of singular integral (kernel function is Formula (8)) for a curved triangular element with source point at the edge of element

Curved surface element	Source point	Gaussian points number CSM	Gaussian points number BTSM	Relative error CSM	Relative error BTSM
Triangular element	(0.6,0.4)	68	68	1.4481e−002	1.6529e−003
		115	115	7.6706e−003	3.0286e−004
		198	198	4.3229e−004	3.4134e−004
		296	296	2.1688e−003	3.5559e−004
		377	377	6.4146e−003	3.5650e−004
		508	508	1.2523e−003	3.5654e−004

Source(s): Created by authors

Table 43. Numerical evaluation of singular integral (kernel function is Formula (9)) for a curved triangular element with source point at the edge of element

Curved surface element	Source point	Gaussian points number CSM	Gaussian points number BTSM	Relative error CSM	Relative error BTSM
Triangular element	(0.6,0.4)	83	83	1.9935e−002	1.5494e−003
		141	141	8.0463e−003	3.6762e−004
		243	243	4.6471e−004	4.1758e−004
		359	359	2.0987e−003	4.3208e−004
		457	457	4.2327e−003	4.3297e−004
		628	628	4.5908e−003	4.3299e−004

Source(s): Created by authors

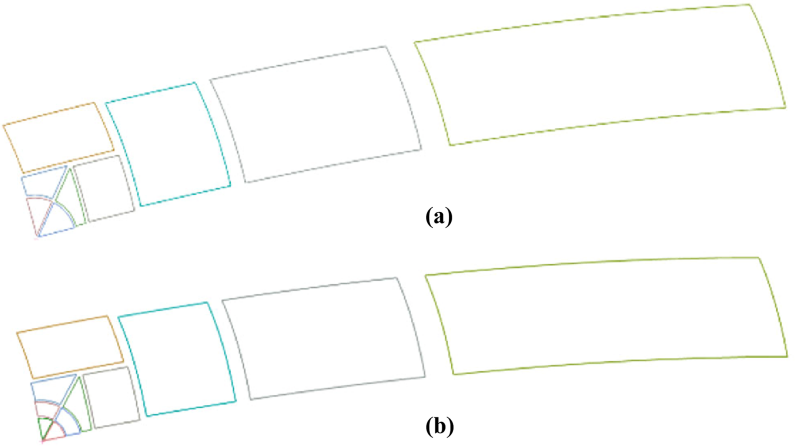

Source(s): Created by authors

Figure 33. Subdivision of a curved quadrilateral element with source point at the vertex of element: (a) The discontinuous kernel function is Formula (8), (b) The discontinuous kernel function is Formula (9)

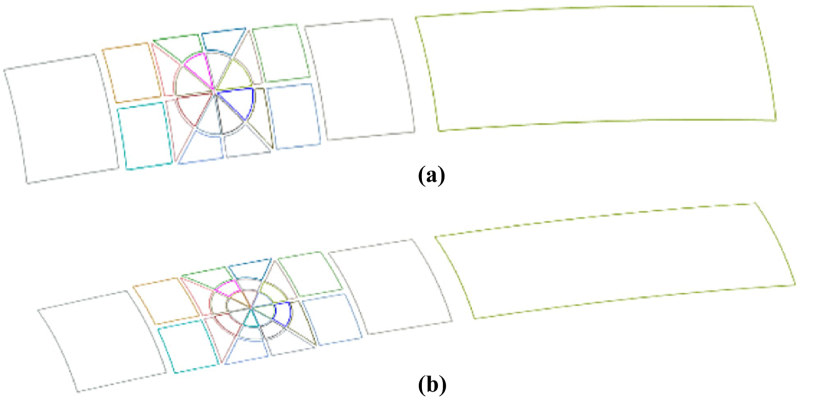

Source(s): Created by authors

Figure 34. Subdivision of a curved quadrilateral element with source point at the interior of element: (a) The discontinuous kernel function is Formula (8), (b) The discontinuous kernel function is Formula (9)

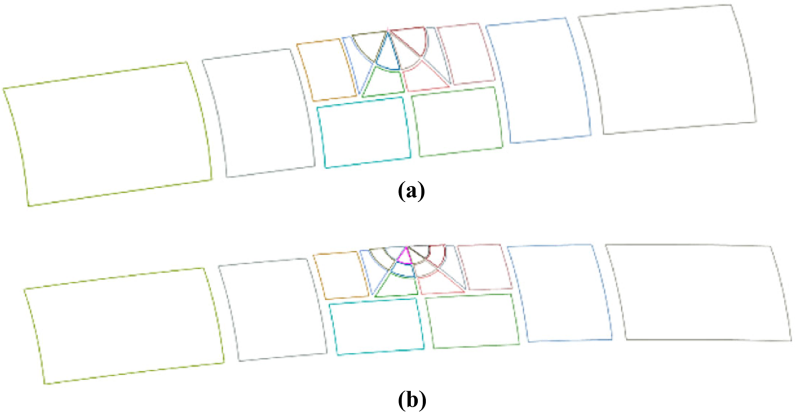

(a)

(b)

Source(s): Created by authors

Figure 35. Subdivision of a curved quadrilateral element with source point at the edge of element: (a) The discontinuous kernel function is Formula (8), (b) The discontinuous kernel function is Formula (9)

Table 44. Numerical evaluation of singular integral (kernel function is Formula (8)) for a curved quadrilateral element with source point at the vertex of element

Curved surface element	Source point	Gaussian points number		Relative error	
		CSM	BTSM	CSM	BTSM
Quadrilateral element	(−1,−1)	48	48	2.4741e−002	6.9451e−004
		82	82	2.3139e−002	3.1283e−004
		123	123	1.0817e−002	3.7229e−004
		200	200	8.4957e−003	3.8568e−004
		273	273	4.5860e−004	3.8632e−004
		373	373	1.2798e−002	3.8635e−004

Source(s): Created by authors

Table 45. Numerical evaluation of singular integral (kernel function is Formula (9)) for a curved quadrilateral element with source point at the vertex of element

Curved surface element	Source point	Gaussian points number		Relative error	
		CSM	BTSM	CSM	BTSM
Quadrilateral element	(−1,−1)	55	55	1.5163e−002	3.7654e−004
		94	94	1.1502e−002	6.1512e−004
		147	147	1.3767e−002	6.7740e−004
		231	231	9.1182e−003	6.9066e−004
		313	313	2.7351e−004	6.9130e−004
		428	428	8.0258e−002	6.9132e−004

Source(s): Created by authors

Table 46. Numerical evaluation of singular integral (kernel function is Formula (8)) for a curved quadrilateral element with source point at the interior of element

Curved surface element	Source point	Gaussian points number		Relative error	
		CSM	BTSM	CSM	BTSM
Quadrilateral element	(−0.5,0)	106	106	2.4589e−002	2.5410e−003
		166	166	1.4374e−002	2.5376e−004
		296	296	2.9444e−003	4.5228e−005
		466	466	6.8647e−003	5.7286e−005
		588	588	1.2566e−003	5.8395e−005
		828	828	8.2116e−003	5.8448e−005

Source(s): Created by authors

Table 47. Numerical evaluation of singular integral (kernel function is Formula (9)) for a curved quadrilateral element with source point at the interior of element

Curved surface element	Source point	Gaussian points number		Relative error	
		CSM	BTSM	CSM	BTSM
Quadrilateral element	(−0.5,0)	134	134	2.1569e−002	2.4540e−003
		214	214	2.6314e−003	2.5354e−004
		392	392	5.6781e−003	4.4181e−005
		590	590	4.0307e−003	5.6008e−005
		764	764	8.8205e−003	5.7078e−005
		1,048	1,048	3.7607e−003	5.7125e−005

Source(s): Created by authors

Table 48. Numerical evaluation of singular integral (kernel function is Formula (8)) for a curved quadrilateral element with source point at the edge of element

Curved surface element	Source point	Gaussian points number		Relative error	
		CSM	BTSM	CSM	BTSM
Quadrilateral element	(0,1)	80	80	3.7274e−003	9.8314e−004
		134	134	5.3713e−003	3.1251e−005
		210	210	3.7735e−004	3.8365e−005
		344	344	2.0180e−002	4.7182e−005
		456	456	7.6579e−003	4.7713e−005
		616	616	8.1346e−004	4.7735e−005

Source(s): Created by authors

Table 49. Numerical evaluation of singular integral (kernel function is Formula (9)) for a curved quadrilateral element with source point at the edge of element

Curved surface element	Source point	Gaussian points number		Relative error	
		CSM	BTSM	CSM	BTSM
Quadrilateral element	(0,1)	94	94	5.0626e−003	9.2031e−004
		158	158	6.8358e−003	8.9984e−006
		258	258	6.3488e−003	8.2713e−005
		406	406	7.4659e−003	9.1475e−005
		544	544	5.3320e−004	9.1995e−005
		726	726	2.0848e−004	9.2014e−005

Source(s): Created by authors

Table 50. Time consumed by evaluating singular integral (kernel function is Formula (8)) for a planer element

Gaussian points number		Relative error		Time (ms)	
CSM	BTSM	CSM	BTSM	CSM	BTSM
123	123	1.7900e−003	7.2420e−004	435	940
185	185	1.5473e−002	1.4993e−005	436	1,180
334	334	7.3122e−003	1.5094e−004	437	1,172
521	521	8.9529e−003	1.5269e−004	442	2,440
644	644	1.6589e−003	1.5453e−004	432	2,962

Source(s): Created by authors

Table 51. Time consumed by evaluating singular integral (kernel function is Formula (9)) for a planer element

Gaussian points number		Relative error		Time (ms)	
CSM	BTSM	CSM	BTSM	CSM	BTSM
145	145	5.5347e−003	7.2802e−004	431	1,041
239	239	5.1805e−002	4.5194e−005	426	1,395
421	421	1.5697e−003	1.2690e−004	428	2,039
635	635	1.5276e−003	1.2898e−004	433	2,886
804	804	3.2573e−003	1.3075e−004	426	3,528

Source(s): Created by authors

Table 52. Time consumed by evaluating singular integral (kernel function is Formula (8)) for a curved element

Gaussian points number		Relative error		Time (ms)	
CSM	BTSM	CSM	BTSM	CSM	BTSM
127	123	5.6584e−004	7.5906e−004	456	931
187	187	2.0397e−002	8.1079e−005	452	1,214
334	334	1.0928e−002	8.6019e−005	455	1,788
529	529	7.5271e−003	8.8453e−005	455	2,575
661	661	1.1995e−003	9.0162e−005	453	3,036

Source(s): Created by authors

EC

Table 53. Time consumed by evaluating singular integral (kernel function is Formula (9)) for a curved element

Gaussian points number		Relative error		Time (ms)	
CSM	BTSM	CSM	BTSM	CSM	BTSM
162	162	8.9128e−003	7.4658e−004	448	1,110
241	241	5.0128e−004	9.2412e−005	456	1,459
433	433	2.7321e−003	8.0883e−005	458	2,195
645	645	1.1275e−004	8.3537e−005	450	2,988
837	837	3.5757e−003	8.5185e−005	450	3,721

Source(s): Created by authors

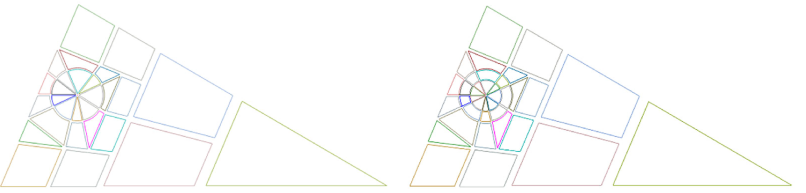

(a) **(b)**

Source(s): Created by authors

Figure 36. Subdivision of a planer element: (a) The discontinuous kernel function is Formula (8), (b) The discontinuous kernel function is Formula (9)

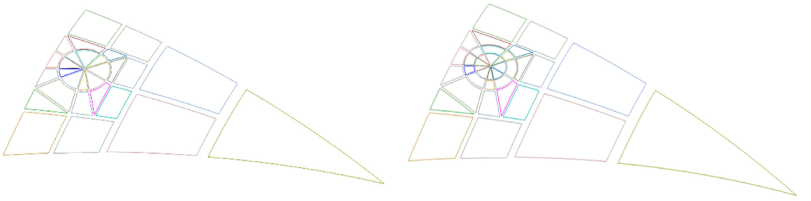

(a) **(b)**

Source(s): Created by authors

Figure 37. Subdivision of a curved element: (a) The discontinuous kernel function is Formula (8), (b) The discontinuous kernel function is Formula (9)

References

Bartoň, M. and Calo, V.M. (2016), "Optimal quadrature rules for odd-degree spline spaces and their application to tensor-product-based isogeometric analysis", *Computer Methods in Applied Mechanics and Engineering*, Vol. 305, pp. 217-240, doi: 10.1016/j.cma.2016.02.034.

Brebbia, C.A., Telles, J.C.F. and Wrobel, L.C. (2012), *Boundary Element Techniques: Theory and Applications in Engineering*, Springer Science & Business Media, New York.

Bu, S. and Davies, T.G. (1995), "Effective evaluation of non-singular integrals in 3D BEM", *Advances in Engineering Software*, Vol. 23 No. 2, pp. 121-128, doi: 10.1016/0965-9978(95)00070-d.

Chen, Y. (2004), "Hypersingular integral equation method for three-dimensional crack problem in shear mode", *Communications in Numerical Methods in Engineering*, Vol. 20 No. 6, pp. 441-454, doi: 10.1002/cnm.685.

Chen, H., Lu, P., Huang, M. and Williams, F. (1998), "An effective method for finding values on and near boundaries in the elastic BEM", *Computers and Structures*, Vol. 69 No. 4, pp. 421-431, doi: 10.1016/s0045-7949(98)00122-9.

Chen, C., He, X. and Huang, J. (2015), "Mechanical quadrature methods and their extrapolations for solving the first kind boundary integral equations of Stokes equation", *Applied Numerical Mathematics*, Vol. 96, pp. 165-179, doi: 10.1016/j.apnum.2015.05.004.

Gao, X.-W. (2010), "An effective method for numerical evaluation of general 2D and 3D high order singular boundary integrals", *Computer Methods in Applied Mechanics and Engineering*, Vol. 199 Nos 45-48, pp. 2856-2864, doi: 10.1016/j.cma.2010.05.008.

Gao, X.W. and Davies, T.G. (2000), "Adaptive integration in elasto-plastic boundary element analysis", *Journal of the Chinese Institute of Engineers*, Vol. 23 No. 3, pp. 349-356, doi: 10.1080/02533839.2000.9670555.

Gao, X.-W., Yang, K. and Wang, J. (2008), "An adaptive element subdivision technique for evaluation of various 2D singular boundary integrals", *Engineering Analysis with Boundary Elements*, Vol. 32 No. 8, pp. 692-696, doi: 10.1016/j.enganabound.2007.12.004.

Guiggiani, M. (1998), "Formulation and numerical treatment of boundary integral equations with hypersingular kernels", *Singular integrals in boundary element methods*, Vol. 10, pp. 85-124.

Hu, J. and Mear, M.E. (2022), "A computational framework for well production simulation: coupling steady state Darcy flow and channel flow by SGBEM–FEM", *Computer Methods in Applied Mechanics and Engineering*, Vol. 399, 115300, doi: 10.1016/j.cma.2022.115300.

Klees, R. (1996), "Numerical calculation of weakly singular surface integrals", *Journal of Geodesy*, Vol. 70 No. 11, pp. 781-797, doi: 10.1007/s001900050067.

Kosinka, J. and Bartoň, M. (2019), "Gaussian quadrature for C1 cubic Clough–Tocher macro-triangles", *Journal of Computational and Applied Mathematics*, Vol. 351, pp. 6-13, doi: 10.1016/j.cam.2018.10.036.

Lachat, J. and Watson, J. (1976), "Effective numerical treatment of boundary integral equations: a formulation for three-dimensional elastostatics", *International Journal for Numerical Methods in Engineering*, Vol. 10 No. 5, pp. 991-1005, doi: 10.1002/nme.1620100503.

Li, S., Mear, M. and Xiao, L. (1998), "Symmetric weak-form integral equation method for three-dimensional fracture analysis", *Computer Methods in Applied Mechanics and Engineering*, Vol. 151 Nos 3-4, pp. 435-459, doi: 10.1016/s0045-7825(97)00199-0.

Liu, Y. (2000), "On the simple-solution method and non-singular nature of the BIE/BEM—a review and some new results", *Engineering Analysis with Boundary Elements*, Vol. 24 No. 10, pp. 789-795, doi: 10.1016/s0955-7997(00)00061-8.

Liu, Y. and Rudolphi, T. (1991), "Some identities for fundamental solutions and their applications to weakly-singular boundary element formulations", *Engineering Analysis with Boundary Elements*, Vol. 8 No. 6, pp. 301-311, doi: 10.1016/0955-7997(91)90043-s.

Liu, Y. and Rudolphi, T. (1999), "New identities for fundamental solutions and their applications to non-singular boundary element formulations", *Computational Mechanics*, Vol. 24 No. 4, pp. 286-292, doi: 10.1007/s004660050517.

Luo, X., Huang, J., Zhu, R. and Wang, C.-L. (2012), "Quadrature methods and their splitting extrapolations for parallel computation of axisymmetric Stokes fluid flow", *Int J Eng Innov Technol*, Vol. 1, pp. 161-168.

Ma, H. and Kamiya, N. (2003), "Nearly singular approximations of CPV integrals with end-and corner-singularities for the numerical solution of hypersingular boundary integral equations", *Engineering Analysis with Boundary Elements*, Vol. 27 No. 6, pp. 625-637, doi: 10.1016/s0955-7997(02)00149-2.

Ma, H., Yin, F. and Qin, Q.H. (2007), "Performance and numerical behavior of the second-order scheme of precise time-step integration for transient dynamic analysis. Numerical Methods for Partial Differential Equations", *International Journal*, Vol. 23 No. 6, pp. 1301-1320, doi: 10.1002/num.20221.

Pin, L. and Haibo, C. (2005), "Singular solutions of anisotropic plate with an elliptical hole or a crack", *Acta Mechanica Solida Sinica*, Vol. 18 No. 2, pp. 130-141.

Provatidis, C. (1998), "A boundary element method for axisymmetric potential problems with non-axisymmetric boundary conditions using fast Fourier transform", *Engineering Computations*, Vol. 15 No. 4, pp. 428-449, doi: 10.1108/02644409810219802.

EC

Rungamornrat, J. and Mear, M.E. (2008a), "A weakly-singular SGBEM for analysis of cracks in 3D anisotropic media", *Computer Methods in Applied Mechanics and Engineering*, Vol. 197 Nos 49-50, pp. 4319-4332, doi: 10.1016/j.cma.2008.05.009.

Rungamornrat, J. and Mear, M.E. (2008b), "Analysis of fractures in 3D piezoelectric media by a weakly singular integral equation method", *International Journal of Fracture*, Vol. 151 No. 1, pp. 1-27, doi: 10.1007/s10704-008-9242-2.

Rungamornrat, J. and Mear, M.E. (2011), "SGBEM–FEM coupling for analysis of cracks in 3D anisotropic media", *International Journal for Numerical Methods in Engineering*, Vol. 86 No. 2, pp. 224-248, doi: 10.1002/nme.3055.

Rungamornrat, J., Sukulthanasorn, N. and Mear, M.E. (2019), "Analysis for T-stress of cracks in 3D anisotropic elastic media by weakly singular integral equation method", *Computer Methods in Applied Mechanics and Engineering*, Vol. 347, pp. 1004-1029, doi: 10.1016/j.cma.2019.01.007.

Sukulthanasorn, N., Watanavit, P., Vo, D., Prasertsri, T., Mear, M.E. and Rungamornrat, J. (2023), "Weakly singular BIE-based procedure for T-stress analysis of cracks in 3D anisotropic linear elastic finite media", *International Journal of Fracture*, Vol. 239 No. 2, pp. 167-188, doi: 10.1007/s10704-022-00667-7.

Telles, J. (1987), "A self-adaptive co-ordinate transformation for efficient numerical evaluation of general boundary element integrals", *International Journal for Numerical Methods in Engineering*, Vol. 24 No. 5, pp. 959-973, doi: 10.1002/nme.1620240509.

Zhang, J., Chi, B., Singh, K.M., Zhong, Y. and Ju, C. (2019b), "A binary-tree element subdivision method for evaluation of nearly singular domain integrals with continuous or discontinuous kernel", *Journal of Computational and Applied Mathematics*, Vol. 362, pp. 22-40, doi: 10.1016/j.cam.2019.04.027.

Zhang, J., Ju, C., Divo, E., Zhong, Y. and Chi, B. (2019a), "A binary-tree subdivision method for evaluation of singular integrals in 3D BEM", *Engineering Analysis with Boundary Elements*, Vol. 103, pp. 80-93, doi: 10.1016/j.enganabound.2019.03.007.

Zhang, J., Lu, C., Zhang, X., Xie, G., Dong, Y. and Li, Y. (2015), "An adaptive element subdivision method for evaluation of weakly singular integrals in 3D BEM", *Engineering Analysis with Boundary Elements*, Vol. 51, pp. 213-219, doi: 10.1016/j.enganabound.2014.11.002.

Zhong, Y., Zhang, J., Dong, Y., Li, Y., Lin, W. and Tang, J. (2016), "A serendipity triangular patch for evaluating weakly singular boundary integrals", *Engineering Analysis with Boundary Elements*, Vol. 69, pp. 86-92, doi: 10.1016/j.enganabound.2016.05.003.

Zhou, F., Li, Y., Zhang, J., Huang, C. and Lu, C. (2015), "A time step amplification method in boundary face method for transient heat conduction", *International Journal of Heat and Mass Transfer*, Vol. 84, pp. 671-679, doi: 10.1016/j.ijheatmasstransfer.2015.01.060.

Corresponding author
Ning Li can be contacted at: lining@triangle.com.cn